Korean J. Chem. Eng., 36(4), 513-521 (2019)
DOI: 10.1007/s11814-019-0236-8

pISSN: 0256-1115
eISSN: 1975-7220

One-pot synthesis of lactic acid from cellulose over a sulfonated Sn-KIT6 catalyst

Weijie Cai*, Qing Chen*, Hao Xuan*, Congming Li, Hao Yu***, Li Cui*, Zhihui Yu*,†, Shaoyin Zhang*, and Fengzuo Qu*,†**

*Faculty of Light Industry and Chemical Engineering, Dalian Polytechnic University, 116023 Dalian, China
**State Key Laboratory Breeding Base of Coal Science and Technology Co-founded by Shanxi Province and the Ministry of Science and Technology, Taiyuan University of Technology, 030024 Taiyuan, China
***College of Chemical and Environmental Engineering, Shandong University of Science and Technology, 266590 Qingdao, China

(*Received 12 November 2018 • accepted 23 January 2019*)

Abstract−A sulfonated Sn-doped KIT-6 catalyst (Sn-KIT-6-Pr-SO_3H) was successfully prepared via the hydrothermal self-assembly method, and its performance towards to value-added lactic acid production from one-pot conversion of renewable cellulose was investigated. Indeed, the physicochemical features of the as-prepared catalysts were deeply characterized by various techniques, including XRD, BET, SEM, FT-IR, XPS, UV-vis and TGA-DSC. The results confirmed its high BET surface area with an ultrahigh cross-linked framework and promising acid strength (co-existence of Brønsted and Lewis acidity). Additionally, the impact of different reaction factors, such as the type of catalysts, temperature, time, recyclability on cellulose conversion and the yield of targeted lactic acid, were determined. Meanwhile, the developed catalyst depicted the promising activity and stability under the optimal reaction conditions. It could be recycled at least four times without any obvious deactivation. This provides insight into developing efficient catalytic systems to convert renewable biomass into value-added chemicals.

Keywords: Lactic Acid, Cellulose, KIT-6, Sulfonation

INTRODUCTION

The efficient conversion of renewable cellulose to bio-derived platform chemicals and/or value-added liquid fuels has been regarded as one of the promising processes for green and sustainable development [1-3]. Among the various derivatives from cellulose conversion, lactic acid (LA) is an attractive building-block chemical that has been widely applied in fields including medicine, cosmetic, and food [4,5]. Particularly, polylactic acid (PLA), a polymerization product of lactic acid, is a type of green, biodegradable polymer to replace conventional fossil fuel-based terephthalate (PET) [6,7]. Herein, the rapidly economic development is expected to accelerate the pilot-scale demand of lactic acid.

To date, lactic acid is mainly obtained via the conventional biofermentation of carbohydrates [8]. In contrast, this biological process was greatly hindered because of the several drawbacks, such as poor scalability, high operation cost and undesirable salt wastes. To address this issue, the development of the chemo-catalytic processes for lactic acid synthesis from the renewable biomass feedstocks has achieved extensive attention in recent years [9]. Indeed, great efforts have been made to explore lactic acid synthesis from monosaccharides such as trioses and hexoses in homogeneous systems and/or heterogeneous ones [10-14]. However, fewer investigations have been conducted for the one-pot production of lactic acid from polysaccharides (e.g., cellulose, hemicellulose) [15,16]. Typically, cellulose, a polymer of D-glucose linked by β-1,4-glycosidic bonds, is the main component of the inedible lignocellulosic biomass, which is highly abundant on the earth [17]. Hence, it is desirable for the direct conversion of cellulose to lactic acid to accelerate the development of the industrial-scale production of bio-based chemicals. Recently, Yan et al. [18] reported that lactic acid might be formed from the hydrothermal treatment of cellulose in the presence of base catalysts such as $Ca(OH)_2$ and/or NaOH. Moreover, Dong et al. [19] found that lactic acid yields as high as 67.6% were reached for cellulose conversion over erbium-exchanged montmorillonite K10 catalyst. In fact, both $ErCl_3$ and Er/b-zeolite catalysts were also developed for the efficient conversion of cellulose to lactic acid in the group of Dong [20,21]. Similarly, catalytic behavior of $Ca(OH)_2$ in lactic acid synthesis from renewable biomass was also deeply evaluated by Sánchez et al. [22]. Wang et al. [23] claimed that a lactic acid yield as high as 68% could be obtained from hydrolysis of ball-milled cellulose (33% crystallinity) catalyzed by $PbCl_2$. In addition, Al^{3+}-Sn^{2+} system was disclosed to efficiently catalyze the direct conversion of cellulose to lactic acid in water [24]. The addition of Zn or Ni promoters greatly accelerated the lactic acid production from cellulose under serious alkaline hydrothermal conditions [25]. Noticeably, satisfactory performance of the homogeneous systems was accompanied by several disadvantages, such as the high difficulty of separation and recovery and/or the serious corrosion for equipment [26,27]. Considering that heterogeneous catalysts might overcome these drawbacks, the conversion of cellulose into lactic acid by heterogeneous catalysis is

†To whom correspondence should be addressed.
E-mail: zhi_hui_yu@163.com, qufz@dlpu.edu.cn

of great interest [28]. For instance, Chambon et al. [29] reported that the tungstated ZrO_2 catalyst with Lewis acidity presented a promising activity on disaccharides conversion, resulting in a 27% lactic acid yield at 190 °C. A similar lactic acid yield was achieved over solid MgO catalyst at 200 °C after 20 h reaction [30]. Although the above developed systems showed relatively good activity in cellulose conversion to lactic acid, one of the main problems was the low stability due to the leaching of active metal species and/or the accumulation deposition of the byproducts over catalyst surface during the reaction process. Herein, the exploitation of the green and highly efficient catalysts for the lactic acid production from cellulose is still a great challenge. Recently, mesoporous SiO_2 based sulfonic solid acid catalysts have been applied in many fields of biomass conversion considering its tunable mesoporous structure and high surface area [31,32]. Guo et al. observed a high HMF yield with SBA-15-SO_3H solid acid catalyst [33], and a similar result over sufonated MCM-41 was reported by Jiang et al. [34]. Another noted feature was that this type of solid catalyst exhibited hydrothermal stability for renewable biomass conversion [35,36].

Herein, we mainly focused on the one-pot synthesis of lactic acid from cellulose over sulfated Sn-KIT6 catalyst (Sn-KIT-6-Pr-SO_3H), which was functionalized with propyl-sulfonic acid groups. The effect of various parameters including reaction temperature, time as well as catalyst recyclability on cellulose conversion to lactic acid was evaluated in detail. Moreover, the relationship between the catalytic behavior and its physicochemical properties was established. The as-prepared Sn-KIT-6-Pr-SO_3H catalyst exhibited an attractive activity and reusability for the lactic acid production from cellulose.

EXPERIMENTAL

1. Materials

Triblock copolymer Pluronic (P123, $EO_{20}PO_{70}EO_{20}$, molecular weight: 5800) was purchased from Shanghai Macklin Biochemical Co., Ltd. (Shanghai, China). Tetraethyl orthosilicate (TEOS, 98.0%), tin chloride pentahydrate ($SnCl_4{\cdot}5H_2O$, 99.0%), hydrochloric acid (HCl, 37%), n-butanol (99.5%), hydrogen peroxide (H_2O_2, 30%) were purchased from Tianjin Kemiou Chemical Reagent Co., Ltd. (Tianjin, China) and used without further purification. Microcrystalline cellulose and 3-mercaptopropyltrimethoxysilane (MPTMS, 95%) were supplied by Shanghai Aladdin Reagent Co., Ltd. (Shanghai, China).

2. Catalyst Preparation

Sn-KIT-6 catalyst was synthesized by hydrothermal technique using TEOS and $SnCl_4{\cdot}5H_2O$ as precursors. First, 5.0 g of P123 was dissolved into a HCl solution (0.5 mol/L, 180 g) at 35 °C, and 5.0 g of n-butanol was slowly added under magnetic stirring. Subsequently, 10.6 g TEOS and an appropriate amount of $SnCl_4{\cdot}5H_2O$ (Si/Sn=40, molar ratio) was added. The obtained mixture was stirred at 35 °C for 24 h and then transferred into a Teflon-lined autoclave for 24 h at 100 °C. After being filtered and dried at 100 °C overnight, the solid product was calcined at 550 °C for 5 h.

The as-prepared Sn-KIT-6 was functionalized with propyl-sulfonic acid groups. Typically, 2.0 g of Sn-KIT-6 was added into an aqueous mixture containing 2.0 mL of MPTMS and 60 mL of dry toluene, and then continuously refluxed at 140 °C for 24 h under N_2 atmosphere. The resulting thiol-functionalized precipitate was thoroughly filtered and extracted using methanol for 12 h at 95 °C. Finally, the thiol group was oxidized to sulfonic group by H_2O_2 (100 mL) overnight. The resulting catalyst was denoted as Sn-KIT-6-Pr-SO_3H. Another reference sulfonated KIT-6 sample without Sn addition was synthesized following the same procedures and labeled as KIT-6-Pr-SO_3H.

3. Catalyst Characterization

X-ray diffraction (XRD) analysis was carried out using a Shimadzu XRD-7000S with Cu $K\alpha$ radiation source operating at 40 kV and 30 mA. N_2 adsorption-desorption isotherms were recorded at −196 °C on 3H-2000PS2 apparatus. The specific surface area, pore size distribution and pore volume were calculated using the (Brunauer-Emmett-Teller) BET and (Barrett-Joyner-Halenda) BJH methods. The morphologies and crystal sizes of catalysts were probed by scanning electron microscopy (SEM) using JEOL JSM-6460LV equipped with energy dispersive X-ray detection. Before scanning, the samples were sprayed on a thin film of gold to enhance conductivity. Fourier transform infrared (FT-IR) spectra were recorded on a Shimadzu IR Prestige-21 spectrometer in the range of 400-4,000 cm^{-1}. X-ray photoelectron spectroscopy (XPS) was performed using an ESCALAB 250 spectrometer equipped with an Mg-Ka X-ray. Thermogravimetric analysis (TG) tests were carried out using a TDA Q50 instrument under a N_2 flow. UV-vis diffuse reflectance spectra were collected on a Shimadzu spectrometer (Model UV-2101 PC) with barium sulfate as reference.

4. Catalytic Tests

Cellulose conversion involved a high-pressure stainless-steel batch reactor (100 mL). Typically, a mixture of cellulose, deionized water and catalyst was added into the autoclave. The vessel was purged by N_2 several times to remove air and the pressure was then charged to 5 MPa using N_2. After reaction, the reactor was quickly placed into ice-water bath and cooled to room temperature. Subsequently, catalyst was separated by filtration and the resulting liquid was analyzed by HPLC (Waters e2695) equipped with a Shodex SUGAR SC1011 column. The operating temperature of column was set at 75 °C and the distilled water was used as mobile phase (0.6 mL/min).

Both cellulose conversion and product selectivity were calculated based on the following equation:

$$X_{cellulose}\% = (\text{moles of reacted cellulose}/\text{moles of initial cellulose}) * 100\%$$

$$S_{product}\% = (\text{moles of carbon in the product}/\text{moles of carbon in the reacted cellulose}) * 100\%$$

5. Catalyst Recyclability

After the reaction, the used catalysts were separated from the solution by centrifugation and thoroughly washed with hot water and dried in the oven at 90 °C over night. The recovered sample was reused for the next run in the same reaction conditions.

RESULTS AND DISCUSSION

1. Physicochemical Features of Catalyst

1-1. XRD

XRD patterns of the investigated catalysts were recorded and

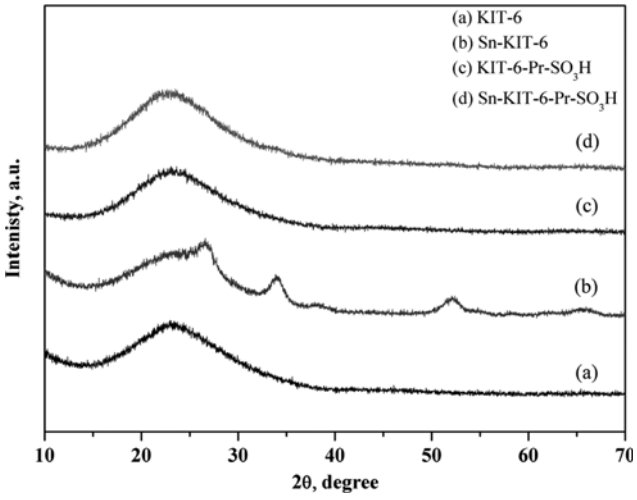

Fig. 1. XRD patterns of samples: (a) KIT-6; (b) Sn-KIT-6; (c) KIT-6-Pr-SO_3H; (d) Sn-KIT-6-Pr-SO_3H.

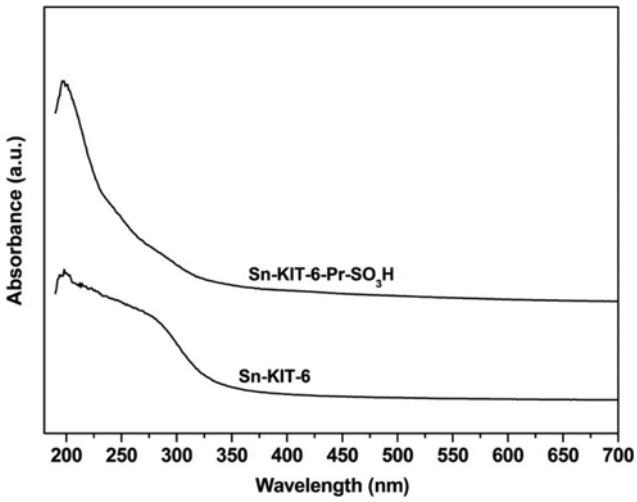

Fig. 2. UV-Vis spectra of the catalysts.

presented in Fig. 1. In all cases, a wide band in the range of 20-30° was assigned to the amorphous nature of SiO_2 [37]. Interestingly, KIT-6-Pr-SO_3H sample exhibited similar patterns in comparison with KIT-6, suggesting that no obvious structure change occurred after the sulfonation process. Noticeably, several shoulders at ca. 26.5, 33.9 and 52.1° in Sn-KIT-6 catalyst were attributed to the crystalline tetragonal SnO_2 (JCPDS Card No. 41-1445), located at the catalyst extra-framework [38]. The calculated crystalline size of SnO_2 was ca. 6.54 nm. After the grafting process, Sn-KIT-6-Pr-SO_3H catalyst still possessed the amorphous structure while the diffraction peaks of SnO_2 species disappeared, indicating that the functionalization with propyl-sulfonic acid groups led to the loss of surface SnO_2 species (extra-framework) as evidenced by the ICP results. As also listed in Table 1, the actual Si/Sn ratio in Sn-KIT-6 sample was ca. 37, which was similar to the targeted value (40). In contrast, a higher Si/Sn ratio (69) was reached for Sn-KIT-6-Pr-SO_3H sample implying the decline of the amount of Sn species.

1-2. UV-vis

Diffuse reflectance UV-vis spectroscopy was collected to figure out the type and coordination states of the incorporated Sn species within the KIT-6 framework. Indeed, metal atoms which isomorphously substituted Si atoms in the framework of KIT-6 need the tetrahedral coordination of silicate units. Hence, its adsorption in UV-vis region was easily discriminated from that of extra-framework species. As presented in Fig. 2, spectra of both containing Sn samples revealed a signal at ca. 203 nm, indicating the presence of Sn^{4+} species with tetrahedral coordination in the KIT-6 framework [39]. In addition, the intensity of this band declined after the sulfonation process, suggesting the loss of Sn species. This was in accordance with the XRD results that the surface Sn species dissolved during the sulfonation period. The broadening feature of Sn-KIT-6 sample was associated with the formation of the Sn species with coordination number more than four (penta- and/or octahedral coordination). With respect to Sn-KIT-6-Pr-SO_3H catalyst, the narrow property and the absence of the adsorption at above 250 nm might exclude the existence of the distorted coordination Sn species and/or small clusters. It was concluded that the dominant Sn species in Sn-KIT-6-Pr-SO_3H sample were tetra-coordinated ones, which normally led to the Lewis acidity. The Lewis acid feature was of great importance for the isomerization of glucose to fructose, which is a critical step for the direct conversion of cellulose to lactic acid.

1-3. BET

The porous structures of the investigated catalysts were determined using N_2 adsorption-desorption isotherms, and the profiles are depicted in Fig. 3. Apparently, all the catalysts possessed relatively high surface areas, with the highest value achieved on the

Table 1. Physicochemical properties of the catalysts

Samples	Si/Sn[a]	S_{BET}[b] ($m^2 \cdot g^{-1}$)	V_p[c] ($cm^3 \cdot g^{-1}$)	d_p[d] (nm)	Total acidity[e] ($mmol \cdot g^{-1}$)
KIT-6	---	618	0.329	2.131	---
Sn-KIT-6	37	576	0.327	2.658	0.491
Sn-KIT-6-Pr-SO_3H	69	509	0.326	3.230	1.608

[a]Actual molar ratio determined by ICP
[b]S_{BET}=BET specific surface area
[c]V_p=Total pore volume
[d]d_P=Pore diameter
[e]Total acidity determined by acid base titration

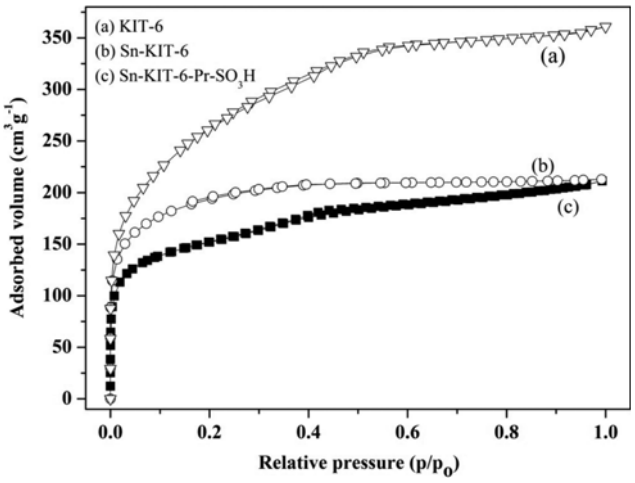

Fig. 3. N_2 adsorption-desorption isotherms of the catalysts.

KIT-6 sample. The modification caused some changes in the shape of the hysteresis loops, which could be attributed to the incorporation of Sn and/or propyl-sulfonic acid groups inside the pore structure of the KIT-6. Meanwhile, both the surface areas and pore volumes decline was ascribed to plugging the pores by doping species and led to them inaccessible for N_2 adsorption. Herein, the blocking of the smaller pores made the increase of average pore sizes, as illustrated by Panpranot et al. [40]. This result indicated that the propyl-sulfonic acid groups might be incorporated into the Sn-KIT-6 structure. In conclusion, the as-prepared Sn-KIT-6-Pr-SO_3H catalyst had relatively higher surface area, which was favorable for the adsorption/conversion of reactants.

1-4. SEM

To check the surface morphology structure, the investigated catalysts were further analyzed by SEM; the results are shown in Fig. 4. Pure KIT-6 (Fig. 3(a)) presented a relatively regular silica spheres with the diameter between 3-5 μm. With respect to Sn-KIT-6 sample, the spherical structure still remained after the doping of Sn species, similar to the results reported by Kishor et al. [41]. Meanwhile, some small white particles (Fig. 3(c)) were observed on the catalyst surface, which were probably ascribed to SnO_2 particles in line with the XRD results. In addition, the element mapping of Sn revealed that Sn species were uniformly distributed over the whole Sn-KIT-6 catalyst surface. However, most of the white species located on the catalyst surface disappeared for Sn-KIT-6-Pr-SO_3H sample, which might be due to the grafting by propyl-sulfonic acid groups. Noticeably, the mapping results also indicated the high dispersion of Sn and S species. Note that the uniform distribution

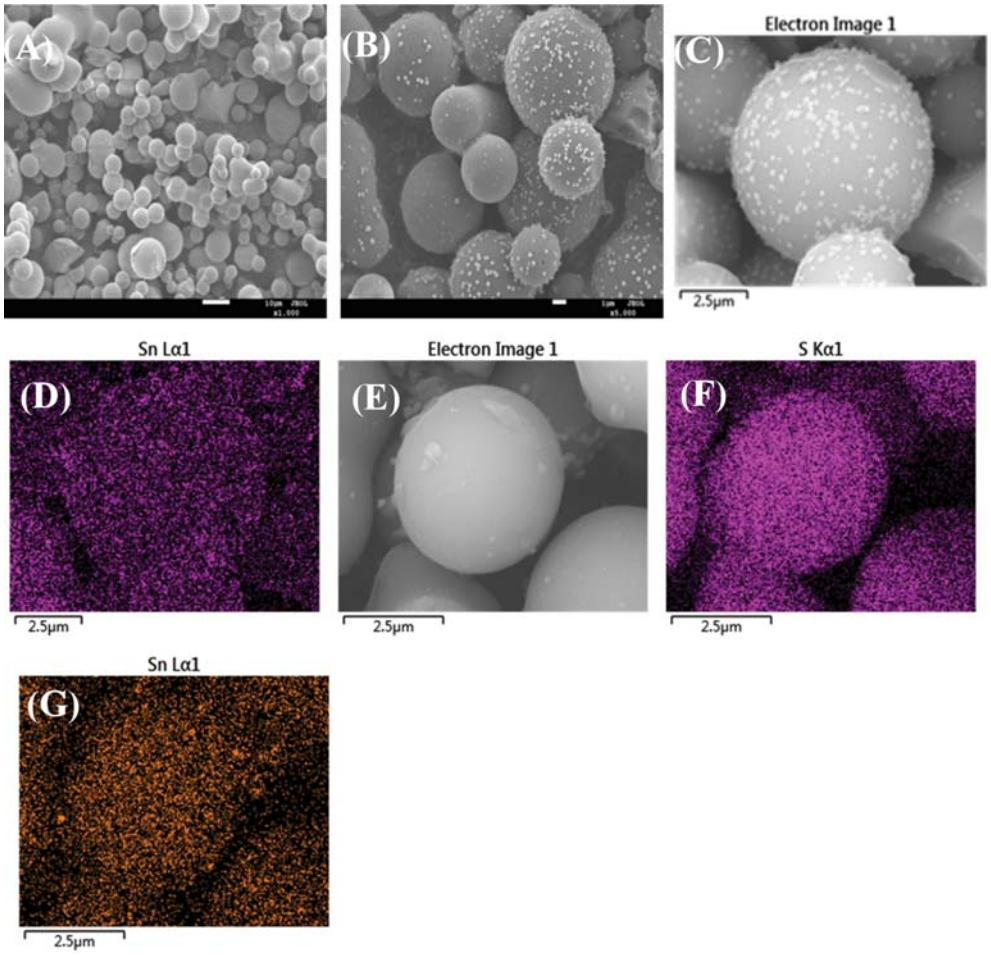

Fig. 4. SEM images and Elemental mapping of KIT-6 (A); Sn-KIT-6 (B)-(D) and Sn-KIT-6-Pr-SO_3H (E)-(G).

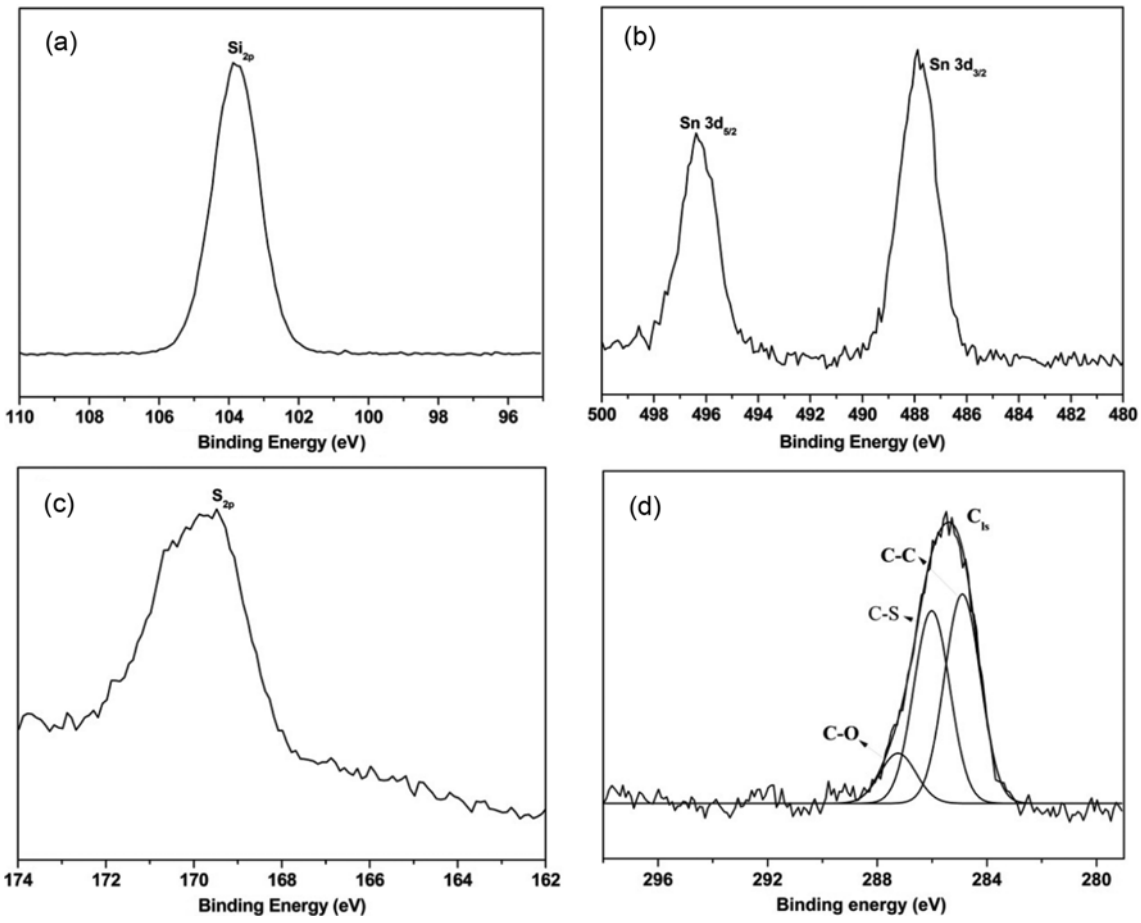

Fig. 5. XPS spectra of Sn-KIT-6-Pr-SO_3H (a) Si_{2p}, (b) Sn_{3d}, (c) S_{2p} and (d) C_{1s}.

of active sites was of great importance to enhance catalyst stability, thereby inhibiting its leaching and/or sintering under the serious reaction conditions.

1-5. XPS

XPS spectra of Sn-KIT-6-Pr-SO_3H catalyst were collected to elucidate the incorporation of sulfonic acid groups and probe the existing states of Sn species. As shown in Fig. 5, a highly resolved band centered at ca. 103.7 eV was assigned to the Si_{2p} signal of the SiO_2 framework. Two symmetric peaks at ca.487.8 and 496.3 eV corresponded to Sn $3d_{5/2}$ and Sn $3d_{3/2}$ of tetrahedrally coordinated framework Sn species and thereby excluded the presence of octahedral coordinated extra-framework species, as pointed out in the previous literature [42,43]. It was accepted that the binding energies of Sn $3d_{5/2}$ and Sn $3d_{3/2}$ for the extra-framework Sn species were located at 486 and 494.4 eV, which are characteristic bands of octahedral Sn species [44]. In fact, the XPS results indicated that the added Sn species were tetrahedrally coordinated in KIT-6 framework in agreement with the UV-vis results. An obvious S_{2p} band was noted at around 169 eV, indicating that S species in Sn-KIT-6-Pr-SO_3H catalyst existed in the type of sulfonic acid groups, as supported by Macia-Agullo et al. [45]. This indicated the occurrence of sulfonation process to form sulfonic acid groups. Moreover, the surface atom ratio of S sites calculated from XPS was ca. 14.2 wt%. Notably, the C_{1s} peak was further deconvoluted into three bands via a Gaussian-type function method. The achieved peaks located at ca. 284.9, 286.1 and 287.2 eV were attributed to the C-C, C-S and C-O bonds, respectively [46]. This further confirmed the successful grafting of the sulfonic acid groups on Sn-KIT6 surface.

1-6. FT-IR

The changes in bonding features induced by the grafting process were monitored by FTIR spectroscopy; the collected spectra are presented in Fig. 6. Obviously, the bending vibration at 450, 810 and 1,088 cm^{-1} corresponded to the symmetric and asymmetric stretching vibrations of Si-O-Si, respectively [38]. Additionally, the bands centered at around 1,644 and 3,400 cm^{-1} were associated with the O-H vibration in adsorbed water molecules, as also discussed by Guo et al. [47]. Indeed, the distinctive peak at ca. 945 cm^{-1} in KIT-6-Pr-SO_3H and Sn-KIT-6-Pr-SO_3H catalyst was attributed to the stretching vibration of Si-O-S, indicating the existence of sulfonic acid species [48]. Meanwhile, the total acidity of KIT-6-Pr-SO_3H and Sn-KIT-6-Pr-SO_3H sample determined by acid-base titration increased to 0.82 and 1.608 $mmol \cdot g^{-1}$ after functionalization of propyl-sulfonic acid groups, which was consistent with the results of FT-IR. On the contrary, the measured total acidity for Sn-KIT-6 catalyst (0.491 $mmol \cdot g^{-1}$) mainly corresponded to the Lewis acid sites. It was reported that Sn sites grafted on ordered silica exhibited Lewis acidity feature [48].

Taking into account the above characterization results, silica

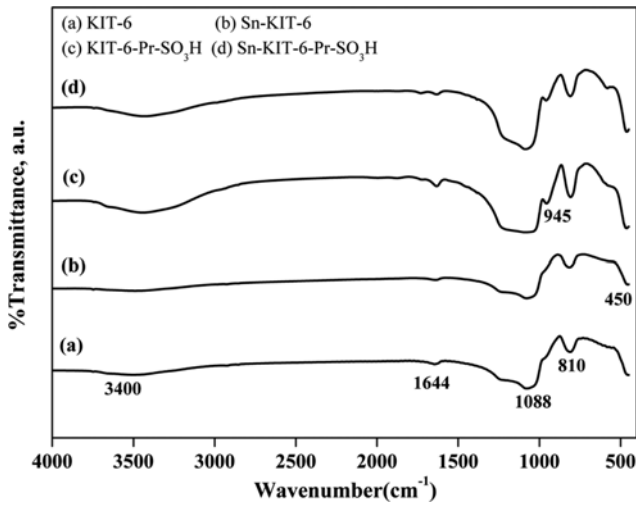

Fig. 6. FT-IR spectra of the investigated catalysts.

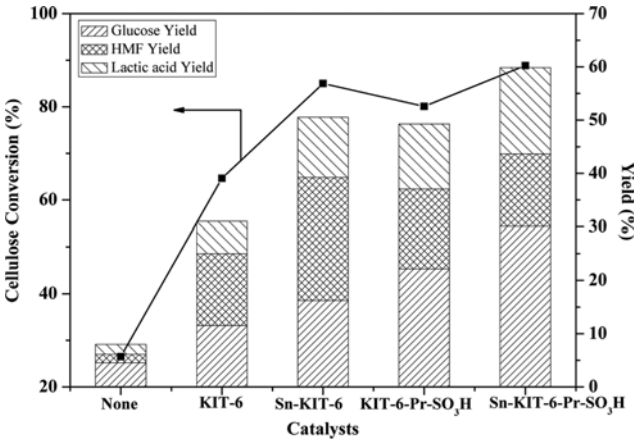

Fig. 8. Effect of catalyst types on cellulose conversion and product yields (Reaction conditions: Catalyst 0.1 g, cellulose 0.3 g, water 30 g, 5 MPa N_2, 210 °C, 1 h).

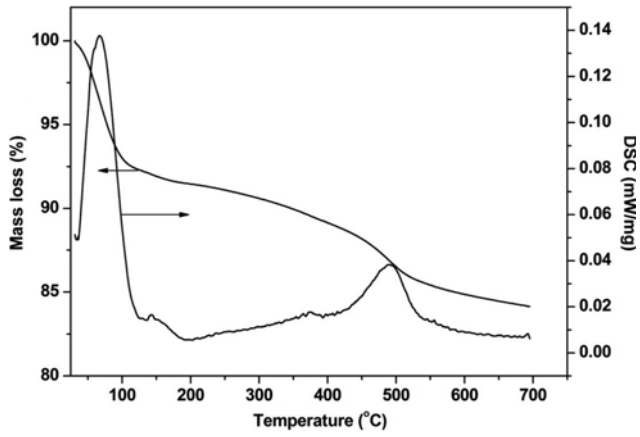

Fig. 7. TGA-DSC curves of Sn-KIT-6-Pr-SO_3H catalyst.

with the condensed framework and a high content of sulfonic acid groups could be synthesized in this work (Sn-KIT-6-Pr-SO_3H). The adequate acid density was regarded as one of the key factors for the catalytic performance of solid acids in biomass value-added conversion.

1-7. TGA-DSC

Considering the industry-scale application, the thermal stability of solid acid catalysts was of great importance. TGA-DSC curve for Sn-KIT-6-Pr-SO_3H catalyst is presented in Fig. 7. First, the weight loss (ca. 8%) in the region of 25-120 °C was caused by the removal of adsorbed water. On the contrary, increasing temperature to 300 °C only resulted in a slight weight loss from 92.1 to 90.8 wt%, indicating the promising thermal stability of the sulfonic acid species confined in KIT-6. This might be favorable for its application as stable sample in renewable biomass conversion, which normally occurs at below 300 °C.

2. Catalytic Performance

2-1. Effect of catalyst Types

Reaction systems with or without catalyst were employed to explore cellulose conversion into lactic acid. As presented in Fig. 8, a negligible yield of lactic acid (ca. 1.9%) was reached under the blank conditions, whereby cellulose conversion was approximately 25% as well as the formation of a small amount of glucose (4.5%) and HMF (1.6%). It was accepted that HMF was formed by the fructose dehydration, which is an isomer of glucose [49]. This result could be ascribed to water autoprotolysis due to the increased ionization constant of hot water, generating H^+ ions for cellulose depolymerization [29]. However, cellulose conversion remarkably increased to 84.4% with the addition of Sn-KIT-6 sample. Simultaneously, the glucose and lactic acid yield also increased to 16.2 and 11.3%, respectively. This result could be attributed to its internal Lewis acidity originating from the tetrahedrally coordinated Sn species, as evidenced by UV-vis and XPS results. The value of Lewis acidity determined by acid-base titration method was around 0.49 mmol·g^{-1} as listed in Table 1. Typically, Lewis acid sites could coordinate with the hydroxyl groups of the depolymerisation intermediates (soluble oligosaccharides, glucose and/or its derivatives) and accelerate cellulose conversion [50]. Li et al. [11]. pointed out that Lewis acid sites promoted the conversion of the intermediate pyruvic aldehyde to lactic acid. Similarly, Chambon et al. proposed that the coordination of solid Lewis sites with the H_3O^+ ions in hot aqueous medium played a critical role in cellulose conversion to lactic acid [29]. For KIT-6-Pr-SO_3H sample with the Brønsted acidity, glucose yield remarkably increased to 22.1% as well as a slight increase of LA yield (12.2%). Meanwhile, conversion of cellulose increased to 80.1%. The observed slight decline of cellulose conversion might be due to the accumulation of humins over catalyst surface, which were easily formed in the presence of strong Brønsted acid sites. Here, when Sn-KIT-6-Pr-SO_3H catalyst was selected, LA yield significantly increased to ca. 16.2% with glucose yield as high as 30.1%, whereas cellulose conversion increased to approximately 88.9%. Concerning its co-existence feature of Brønsted and Lewis acidity, the experimental results indicated that the type of catalyst acidity played an important role in LA production from cellulose hydrolysis. Based on the previous knowledge, moderate amounts of Brønsted acid sites could enhance cellulose hydrolysis [51] and Lewis acidity might lead to the occurrence of glucose

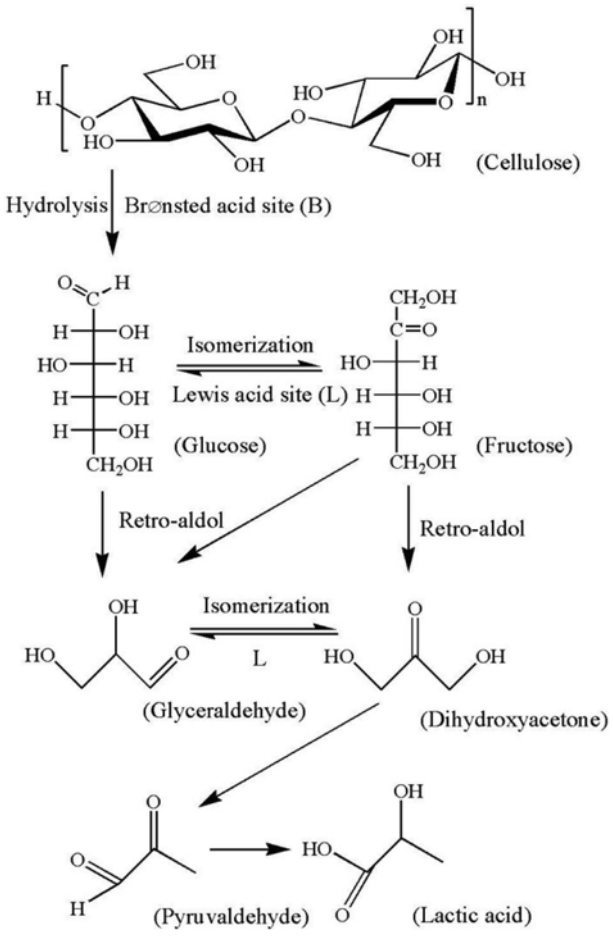

Scheme 1. Reaction mechanism of lactic acid formation from one-pot conversion of cellulose.

isomerization to fructose followed by a series of retro-aldol condensation and isomerization reactions to form lactic acid [52]. Note that the decline of HMF yield was related to the excess acidity which promoted the subsequent conversion of HMF into levulic acid and/or humins.

Hence, it might be deduced that lactic acid production from direct cellulose conversion contained multiple reaction steps including C-C bond cleavage. A possible reaction mechanism is depicted in Scheme 1. First, cellulose depolymerized into glucose catalyzed by Brønsted acid sites, and the isomerization of glucose to fructose occurred in the presence of Lewis acid sites. The formed fructose subsequently underwent retro-aldol fragmentation to dihydroxyacetone (DHA) and glyceraldehyde (GLY). Finally, the formed DHA and/or GLY species were converted to lactic acid via the dehydration and isomerization reactions. For the investigated Sn-KIT-6-Pr-SO_3H catalyst, Lewis acidity was provided by tetrahedrally coordinated Sn species within the silica framework, whereas Brønsted acidity was attributed to the introduction of sulfonic acid groups. The presence of both types of acid sites was critical for the selective conversion of the mentioned intermediates (DHA and/or GLY) into lactic acid. Therefore, it was concluded that the cooperation effect between the Lewis acid sites and the Brønsted acid sites played an important role in the formation of lactic acid from cellulose.

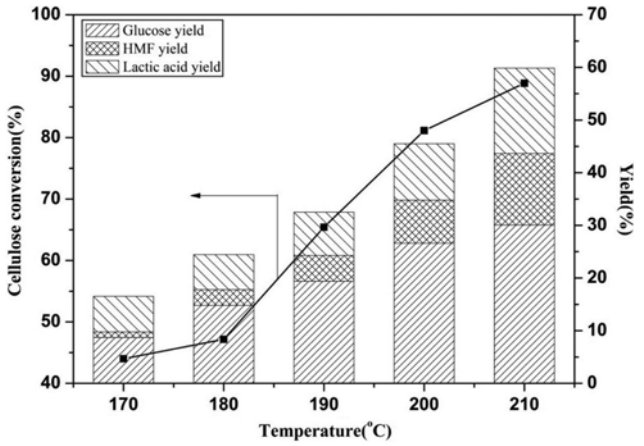

Fig. 9. The influence of reaction temperature on lactic acid production from cellulose (Reaction conditions: Catalyst 0.1 g, cellulose 0.3 g, water 30 g, 5 MPa N_2, 1 h).

2-2. Optimization of Reaction Parameters

Based on the above discussion, Sn-KIT-6-Pr-SO_3H was selected as the model catalyst to determine the impact of various reaction conditions in the following trial.

2-2-1. Temperature Influence

The influence of reaction temperature on cellulose conversion and the targeted LA yield was investigated in detail; the results are presented in Fig. 9. Here, for heating temperature from 170 to 210 °C, cellulose conversion remarkably increased from 44 to 89%, and the yield of lactic acid was also enhanced from 6.7 to 16.2%. The achieved yield of another product glucose increased from 8.7 to 30.1%. Simultaneously, the selectivity of side-product HMF was improved upon heating. The power design limit of the batch reactor hindered the further investigation under the higher temperature region. Notably, the maximum cellulose conversion and LA yield was reached at 210 °C under the same reaction time. In addition, it was accepted that the lower temperature easily resulted in the formation of polymer-like chemicals and/or intermediates as previously illustrated by Shen et al. [53]. Considering this factor, 210 °C was selected as the optimal temperature to further determine the effect of other factors on the catalytic performance.

2-2-2. Reaction Time Influence

The effect of reaction time is summarized in Fig. 10. When the tests were conducted at 210 °C for 0.5 h, cellulose conversion was around 70.4% and the LA yield was 13.5% as well as the glucose yield of 30%. Upon prolonging the time to 1 h, both cellulose conversion and LA selectivity reached the maximum value with the results of 88.9% and 16.2% respectively. However, further increasing the time caused the decline of cellulose conversion. This phenomenon might not reveal the decrease of catalyst activity. Probably, both the polymerization of intermediates including HMF, glucose, etc., and the partial carbonation of cellulose could form the humins, which might also be regarded as "the unreacted cellulose" leading to the calculation error. This was indirectly supported by the observed decline of HMF (from 8.9 to 0.47%) and/or glucose yields (from 30.6 to 17.5%). In contrast, only a slight decline (from 16.2 to 14.6%) of LA yield was noted after a reaction of 2.5 h, confirm-

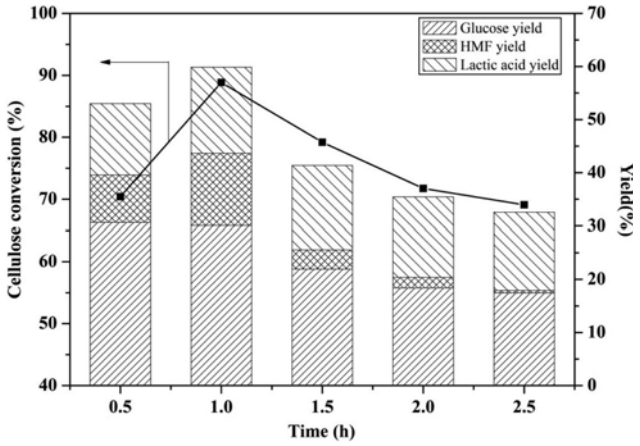

Fig. 10. Effect of reaction time on lactic acid production from cellulose (Reaction conditions: Catalyst 0.1 g, cellulose 0.3 g, water 30 g, 5 MPa N_2, T: 210 °C).

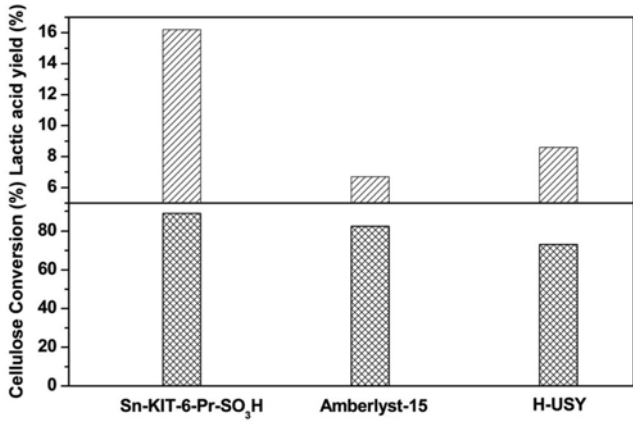

Fig. 11. Comparison of Sn-KIT-6-Pr-SO_3H catalyst with model commercial solid acid catalysts (Reaction conditions: Catalyst 0.1 g, cellulose 0.3 g, water 30 g, 5 MPa N_2, time 1 h, T: 210 °C).

ing that lactic acid was stable at 210 °C and overreaction of the lactic acid was negligible.

Other two-model commercial solid acid catalysts (H-USY, Amberlyst-15) were selected and evaluated for one-pot conversion of cellulose to lactic acid under the above determined optimal conditions. The results are in Fig. 11. For Amberlyst-15 sample, LA yield was only around 6.7% and cellulose conversion was 82.5%. H-USY exhibited cellulose conversion of 73.1% and LA yield of 8.6%. This result revealed that the as-prepared Sn-KIT-6-Pr-SO_3H catalyst had better catalytic behavior than that of the conventional solid acid samples.

2-3. Recycling Capcacity of Sn-KIT-6-Pr-SO_3H Catalyst

Catalyst stability is critical for the potentially industrial-scale application to reduce operation cost. It was elucidated that the conventional Lewis acid catalysts, such as $SnCl_4$, $TiCl_4$ etc., were easily deactivated and/or decomposed under the severe hydrothermal conditions, which made it difficult to recover and reuse these catalysts after reactions [54,55]. To address this issue, stability tests of Sn-KIT-6-Pr-SO_3H catalyst were further conducted. As depicted in

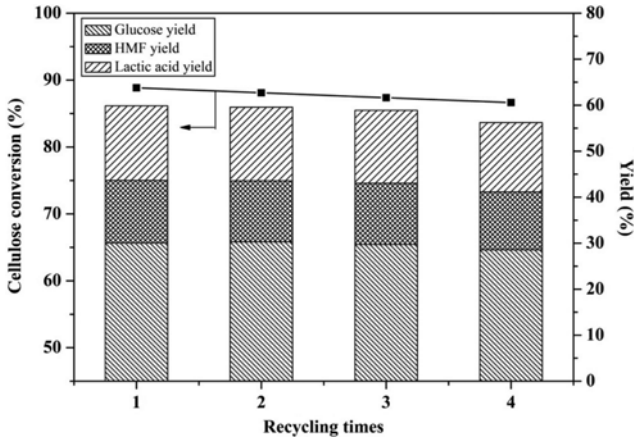

Fig. 12. Recycling of Sn-KIT-6-Pr-SO_3H catalyst for lactic acid formation from cellulose conversion (Reaction conditions: Catalyst 0.1 g, cellulose 0.3 g, water 30 g, 5 MPa N_2, time 1 h, T: 210 °C).

Fig. 12, only a slight decrease of cellulose conversion (from 88.9% to 86.6%) and the yield to LA (from 16.2% to 15.1%) was observed after four consecutive catalytic runs, which was ascribed to the occupation of the active sites by the humins and/or the slight leaching of acidic species [56,57]. We concluded that the investigated Sn-KIT-6-Pr-SO_3H catalyst was easily recycled without any noticeable deactivation. Therefore, the developed Sn-KIT-6-Pr-SO_3H catalyst in this work might be a promising alternative for water resistant solid acid catalyst in value-added chemical production from renewable biomass conversion.

CONCLUSIONS

A well-ordered sulfonated Sn-KIT-6 catalyst with high specific surface area, ultrahigh cross-linked framework, and the promising acid strength was successfully synthesized via the hydrothermal self-assembly technique. The as-prepared Sn-KIT-6-Pr-SO_3H catalyst exhibited high efficiency and remarkable recyclability in lactic acid production from one-pot conversion of cellulose. It depicted cellulose conversion of 88.9% and LA yield of 16.2% under the optimal reaction conditions. Comparable yields of the targeted lactic acid were reached even after four consecutive cycles. Additionally, its catalytic behavior was much better than that of the conventional commercial solid acid catalysts (like Amberlyst15, H-USY). Hence, this work could develop a sustainable and low cost process to synthesize highly efficient and stable silica-based solid acids for the depolymerization of renewable crystalline cellulose into value-added chemicals.

ACKNOWLEDGEMENTS

This work was supported by Natural Science Foundation of Liaoning Province (20170540073), General project from Department of education of Liaoning Province (2017J026), National Key R&D Program of China (2017YFB0308701), Natural Science Foundation of Liaoning Province (20170520427).

REFERENCES

1. X. Mei, J. Liu, W. Fu, T. Tang and D. Wu, *ACS Sustainable. Chem. Eng.*, **5**, 5800 (2017).
2. S. S. Kim, H. V. Ly, B. H. Chun, J. H. Ko and J. Kim, *Korean J. Chem. Eng.*, **33**, 3128 (2016).
3. J. D. Zhu, L. H. Gan, B. X. Li and X. Yang, *Korean J. Chem. Eng.*, **34**, 110 (2017).
4. R. A. Oliveira, A. Komesu, C. E. V. Rossell and R. M. Filho, *Biochem. Eng. J.*, **133**, 219 (2018).
5. A. J. Ryu, T. Y. Kim, D. S. Yang, J. H. Park and J. J. Jeong, *Korean J. Chem. Eng.*, **35**, 1673 (2018).
6. O. Oguz, K. Bilge, E. Simsek, M. K. Citak, A. A. Wis, G. Ozkoc and Y. Z. Menceloglu, *Ind. Eng. Chem. Res.*, **56**, 8568 (2017).
7. C. M. Tang, J. S. Peng, X. L. Li, Z. J. Zha, H. J. Gao, W. Bai, N. Jiang and Y. W. Liao, *Korean J. Chem. Eng.*, **33**, 99 (2016).
8. A. S. Qureshi, J. A. Zhang, L. C. Sousa and J. Bao, *ACS Sustainable. Chem. Eng.*, **5**, 9254 (2017).
9. P. Wattanapaphawong, P. Reubroycharoen and A. Yamaguchi, *RSC Adv.*, **7**, 18561 (2017).
10. K. Nakajima, J. Hirata, M. Kim, N. K. Gupta, T. Murayama, A. Yoshida, N. Hiyoshi, A. Fukuka and W. Ueda, *ACS Catal.*, **8**, 283 (2018).
11. L. Li, X. Collard, A. Bertrand, B. F. Sels, P. P. Pescarmona and C. Aprile, *J. Catal.*, **314**, 56 (2014).
12. L. Y. Li, F. Shen, R. L. Smith and X. H. Qi, *Green. Chem.*, **19**, 76 (2017).
13. M. S. Holm, S. Saravanamurugan and E. Taarning, *Science*, **328**, 602 (2010).
14. M. S. Holm, Y. J. Pagán-Torres, S. Saravanamurugan, A. Riisager, J. A. Dumesic and E. Taarning, *Green. Chem.*, **14**, 702 (2012).
15. W. P. Deng, Q. H. Zhang and Y. Wang, *Catal. Today*, **234**, 31 (2014).
16. L. S. Yang, J. Su, S. Carl, J. G. Lynam, X. K. Yang and H. F. Lin, *Appl. Catal. B.*, **162**, 149 (2015).
17. G. Z. Wang, X. F. Tan, H. Lv, M. M. Zhao, M. Wu, J. P. Zhou, X. M. Zhang and L. N. Zhang, *Ind. Eng. Chem. Res.*, **55**, 5263 (2016).
18. X. Y. Yan, F. M. Jin, K. Tohji, A. Kishita and H. Enomoto, *AIChE J.*, **56**, 2727 (2010).
19. X. Lei, F. F. Wang, C. L. Liu, R. Z. Yang and W. S. Dong, *Appl. Catal. A.*, **482**, 78 (2014).
20. F. F. Wang, J. Liu, H. Li, C. L. Liu, R. Z. Yang and W. S. Dong, *Green. Chem.*, **17**, 2455 (2015).
21. H. Z. Wu, H. F. Ren, C. L. Liu, C. L. Xu and W. S. Dong, *J. Porous. Mater.*, **24**, 697 (2017).
22. C. Sánchez, A. García, R. Llano-Ponte and J. Labidi, *Chem. Eng. J.*, **181-182**, 655 (2012).
23. Y. L. Wang, W. P. Deng, B. J. Wang, Q. H. Zhang, X. Y. Wan, Z. C. Tang, Y. Wang, C. Zhu, Z. X. Cao, G. C. Wang and H. L. Wan, *Nat. Commun.*, **4**, 2141 (2013).
24. W. P. Deng, P. Wang, B. J. Wang, Y. L. Wang, L. F. Yang, Y. Y. Li, Q. H. Zhang, Z. X. Cao and Y. Wang, *Green. Chem.*, **20**, 735 (2018).
25. S. Zhang, F. Jin, J. Hu and Z. Huo, *Bioresour. Technol.*, **102**, 1998 (2011).
26. S. Tolborg, I. Sadaba, C. M. Osmundsen, P. Fristrup, M. S. Holm and E. Taarning, *Chem. Sus. Chem.*, **8**, 613 (2015).
27. A. G. Daful and J. F. Görgens, *Chem. Eng. Sci.*, **162**, 53 (2017).
28. D. Verma, R. Insyani, Y. W. Suh, S. M. Kim and J. Kim, *Green. Chem.*, **19**, 1969 (2017).
29. F. Chambon, F. Rataboul, C. Pinel, A. Cabiac, E. Guillon and N. Essayem, *Appl. Catal. B*, **105**, 171 (2011).
30. Z. Liu, W. Li, C. Pan, P. Chen, H. Lou and X. Zheng, *Catal. Commun.*, **15**, 82 (2011).
31. T. N. Ng, X. Q. Chenac and K. L. Yeung, *RSC Adv.*, **5**, 13331 (2015).
32. X. Chen, M. Arruebo and K. L.Yeung, *Catal. Today*, **204**, 140 (2013).
33. X. Guo, Q. Cao, Y. Jiang, J. Guan, X. Wang and X. Mu, *Carbohydr. Res.*, **351**, 35 (2012).
34. C. W. Jiang, A. X. Su and X. M. Li, *Adv. Mater. Res.*, **396**, 1190 (2011).
35. H. F. Xiong, H. N. Pham and A. K. Datye, *Green. Chem.*, **16**, 4627 (2014).
36. Q. Pan, A. Ramanathan, W. K. Snavely, R. V. Chaudhari and B. Subramaniam, *Ind. Eng. Chem. Res.*, **52**, 15481 (2013).
37. H. X. Cao, J. Zhang, C. L. Guo, J. G. Chen and X. K. Ren, *Chin. J. Catal.*, **38**, 1127 (2017).
38. R. Rajalakshmia, R. Maheswaria and A. Ramanathanb, *Mater. Res. Bull.*, **75**, 224 (2016).
39. K. Chaudhari, T. K. Das, P. R. Rajmohanan, K. Lazar, S. Sivasanker and A. J. Chandwadkar, *J. Catal.*, **183**, 281 (1999).
40. J. Panpranot, J. G. Goodwin and A. Sayari, *Catal. Today*, **77**, 269 (2002).
41. R. Kishor and A. K. Ghoshal, *Micropor. Mesopor. Mat.*, **242**, 127 (2017).
42. E. H. Yuan, W. L. Dai, G. J. Wu, N. J. Guan, M. Hunger and L. D. Li, *Micropor. Mesopor. Mat.*, **270**, 265 (2018).
43. W. N. P. van der Graaff, G. N. Li, B. Mezari, E. A. Pidko and E. J. M. Hensen, *Chem. Cat. Chem.*, **7**, 1152 (2015).
44. M. P. Pachamuthu, K. Shanthi, R. Luque and A. Ramanathan, *Green. Chem.*, **15**, 2158 (2013).
45. J. A. Macia-Agullo, M. Sevilla, A. Diez and A. B. Fuertes, *Chem. Sus. Chem.*, **3**, 1352 (2010).
46. Q. Wu, F. J. Liu, X. F. Yi, Y. C. Zou and L. L. Jiang, *Green. Chem.*, **20**, 1020 (2018).
47. Y. H. Guo, C. Xia and B. S. Liu, *Chem. Eng. J.*, **237**, 421 (2014).
48. A. Corma, M. T. Navarro and M. Rene, *J. Catal.*, **219**, 242 (2003).
49. H. Zhao, J. E. Holladay, H. Brown and Z. C. Zhang, *Science*, **316**, 1597 (2007).
50. F. F. Wang, C. L. Liu and W. S. Dong, *Green. Chem.*, **15**, 2091 (2013).
51. L. Hu, L. Lin, Z. Wu, S. Y. Zhou and S. J. Liu, *Appl. Catal. B.*, **174-175**, 225 (2015).
52. E. Taarning, S. Saravanamurugan, M. S. Holm, J. Xiong and R. M. West, *Chem. Sus. Chem.*, **2**, 625 (2009).
53. L. Q. Shen, X. Zhou, A. L. Wang, H. B. Yin, H. X. Yin and W. J. Cui, *RSC Adv.*, **7**, 30725 (2017).
54. S. Kobayashi, M. Sugiura, H. Kitagawa and W. W. L. Lam, *Chem. Rev.*, **102**, 2227 (2002).
55. L. Peng, L. Lin, J. Zhang, J. Zhuang, B. Zhang and Y. Gong, *Molecules*, **15**, 5258 (2010).
56. A. Prabhu, L. Kumaresan, M. Palanichamy and V. Murugesan, *Appl. Catal. A.*, **360**, 59 (2009).
57. Y. Zhang, J. Wang, J. Ren, X. Liu, X. Li, Y. Xia, G. Lu and Y. Wang, *Catal. Sci. Technol.*, **2**, 2485 (2012).